sustainability

MDPI

Article

Development of Sustainable Cement-Based Materials with Ultra-High Content of Waste Concrete Powder: Properties and Improvement

Ruihan Hu, Youchao Zhang *, Zhiyu Zhang and Zhiming Ma *

College of Architectural Science and Engineering, Yangzhou University, Yangzhou 225127, China; rui_han_hu@163.com (R.H.); yz_zhangzy@163.com (Z.Z.)
* Correspondence: zhangyouchao@yzu.edu.cn (Y.Z.); 006879@yzu.edu.cn (Z.M.)

Abstract: The recycled powder (RP) of construction waste, as a kind of silica–aluminum waste, can have a certain gelling effect after alkali activation modification. Sodium silicate (water glass) and NaOH are used as composite alkali activators to stimulate RP to prepare alkali-activated mortar. The different micro and macro properties of RP are studied under the ultra-high substitution rates of 70%, 80%, 90%, and 100% of cementation-based materials. The results show that the mechanical properties of the regenerated powder mixture decrease gradually with the increase in the substitution rate. When the replacement rate of RP is 70%, the 3 d and 28 d compressive strength decreases by 73.63% and 69.46%, respectively. When the replacement rate reaches 100%, the 3 d and 28 d compressive strength decreases by 96.98% and 93.74%, respectively. The cement-based material after alkali excitation has the characteristics of early strength and the mechanical properties are greatly improved, and the mechanical properties of cement-based materials can be effectively increased by increasing the modulus of water glass. At 70%RP substitution rate, the compressive strength of 28 d increases by 3.59% and 107.71% when the modulus of sodium silicate is 1.0 M and 1.6 M, compared with the unactivated groups. At 100%RP substitution rate, the 28 d strength of the unexcited specimen is 0.92 MPa, and the 28 d compressive strength reaches 6.15 MPa and 12.86 MPa when the modulus of sodium silicate is 1.0 M and 1.6 M. The results show that the alkali-activated mortar has good application potential.

Keywords: alkali-activated mortar; recycled powder; microstructure; ultra-high replacement rate

check for updates

Citation: Hu, R.; Zhang, Y.; Zhang, Z.; Ma, Z. Development of Sustainable Cement-Based Materials with Ultra-High Content of Waste Concrete Powder: Properties and Improvement. *Sustainability* **2023**, *15*, 14812. https://doi.org/10.3390/su152014812

Academic Editor: Syed Minhaj Saleem Kazmi

Received: 16 September 2023
Revised: 1 October 2023
Accepted: 10 October 2023
Published: 12 October 2023

1. Introduction

Concrete is the most widely used construction material in the world, and with the rapid development of infrastructure and urbanization in China, the amount of construction waste generated has been increasing year by year. Improper disposal of this waste can have negative environmental impacts [1,2]. Therefore, effective utilization of construction waste [3,4] can not only alleviate natural resource shortages but also contribute to environmental protection, optimizing resource allocation and promoting sustainable economic and social development. Researchers have proposed using recycled aggregates (RAs) or recycled powder (RP) as replacements for natural aggregates and ordinary Portland cement (OPC), which can have a positive impact on reducing the environmental impact of cement [5–7]. After screening and crushing, concrete generates approximately 10–20% of construction waste powder, which can be used as a substitute for OPC in the binding process. Researchers have produced eco-friendly concrete by grinding RP into fine particles [8]. The main chemical components of RP are SiO_2, $CaCO_3$, and Al_2O_3, which have potential volcanic activity and can be used as filling materials after alkali activation [9,10]. The addition of RP reduces the fluidity of the mixture and decreases the self-shrinkage performance of cement-based materials [11]. Due to the presence of inert quartz and calcite in RP, hydration is generally not easy. When RP is added in experiments, the average pore size of

the obtained test block increases, and the mechanical properties generally decrease [12–14]. In addition, the inclusion of RP increases water ingress and chloride migration in concrete [15,16]. Researchers have studied the optimal proportion and performance of RP in concrete and used carbonation curing to improve its performance, which can absorb CO_2 gas [17]. Additionally, researchers have found that the activation of RP can be improved by thermal treatment, which involves thermally activating RP at 600–800 °C to achieve optimal performance [18,19]. During the thermal activation process, active calcium silicate and calcium oxide are generated [20]. Through the utilization of construction waste, the use of conventional raw materials in conventional materials is reduced [21–23]. The addition of nanomaterials or fibers to the material can optimize its strength and durability [24–26]. Currently, researchers are exploring the use of construction waste as a binding material to produce environmentally friendly geopolymer [27–29]. The use of materials prepared from construction waste has a positive effect on environmental protection and reduces the amount of Portland cement and fly ash used [30]. For example, waste glass powder [31,32] and waste ceramic tiles and brick powder from construction and demolition waste [33] can be reused as sustainable polymer adhesives, and previous studies have reported some satisfactory results. The high replacement rate of recycled powders and water glass in the preparation of cement-based materials has received little attention in previous studies. Compared with other related experiments, the innovation of this experiment lies in the use of ultra-high-substitution-rate RP to replace cement, and the study of the impact of different substitution rates on cement-based materials at PR substitution rates of 70%, 80%, 90%, and 100%. Another innovation is the quantification of the impact of different modulus on the macroscopic and microscopic characterization of cement-based materials with different substitution rates of RP, providing necessary data for further research and utilization of RP and alkali activators in geopolymers. Therefore, this paper studied the performance of RP mixtures with high substitution rates, as well as the modification ability of alkali activators on their micro- and macro properties, proving the feasibility of using RP as a cementitious material to prepare ultra-high content of alkali-activated mortar. The findings of this study will provide a further basis for the utilization and promotion of RP.

2. Materials and Methods

To reduce the high CO_2 emissions associated with ordinary Portland cement (OPC), the generated construction waste powder was processed into recycled powder (RP) after the concrete was collected and broken. These powders were mixed with sodium silicate solution to prepare cement-based materials. The cement-based materials were then cured in a standard procedure until reaching the curing time required for testing their microstructure, mechanical properties, and resistance to chloride diffusion.

2.1. Raw Materials and Experimental Scheme

The experimental process is shown in Figure 1a. By collecting and crushing concrete construction waste, the generated construction waste powder was ground into RP, and RP ($\leq$150 μm) was used to replace OPC with an ultra-high substitution rate to prepare sustainable cement-based materials while an alkali activator was used to improve the performance of ultra-high-content RP cementing materials. Finally, the micro-characteristics, mechanical strength, water transport, and chloride ingress of cement-based materials were determined.

The RP was used as the binder material to replace the OPC in the experiment, with a replacement rate of up to 100%. The impact of the replacement rate in the experiment was discussed, with CBM-70, CBM-80, CBM-90, and CBM-100 representing the use of RP to replace cement with 70%, 80%, 90%, and 100% replacement rates, respectively.

The particle size of RP is shown in Figure 2a, with a median particle size of 17.60 μm. Figure 2b shows that the recycled powder has an irregular microstructure, with larger particles often surrounded by many small particles. Moreover, SEM images show large pieces of C-S-H. Figure 2c shows the XRD mineral composition of RP. The highest content of calcite in the recycled powder is derived from the coarse aggregate in the parent material

or the concrete waste hydration products in the construction waste. Additionally, a large proportion of silicon dioxide and calcite are present. It also contains large pieces of hydrated calcium silicate, some unhydrated cement particles, and high-strength inert quartz and calcite, making it difficult to participate in new hydration reactions. Figure 2d shows the infrared spectra of RP, where a significant absorption peak in the silicon–oxygen stretching vibration is observed around 970 cm^{-1}, indicating a higher proportion of hydrated calcium silicate in RP. The maximum C-O stretching vibration absorption peak indicates a high content of calcium carbonate in RP, CH crystals, and quartz and calcite particles.

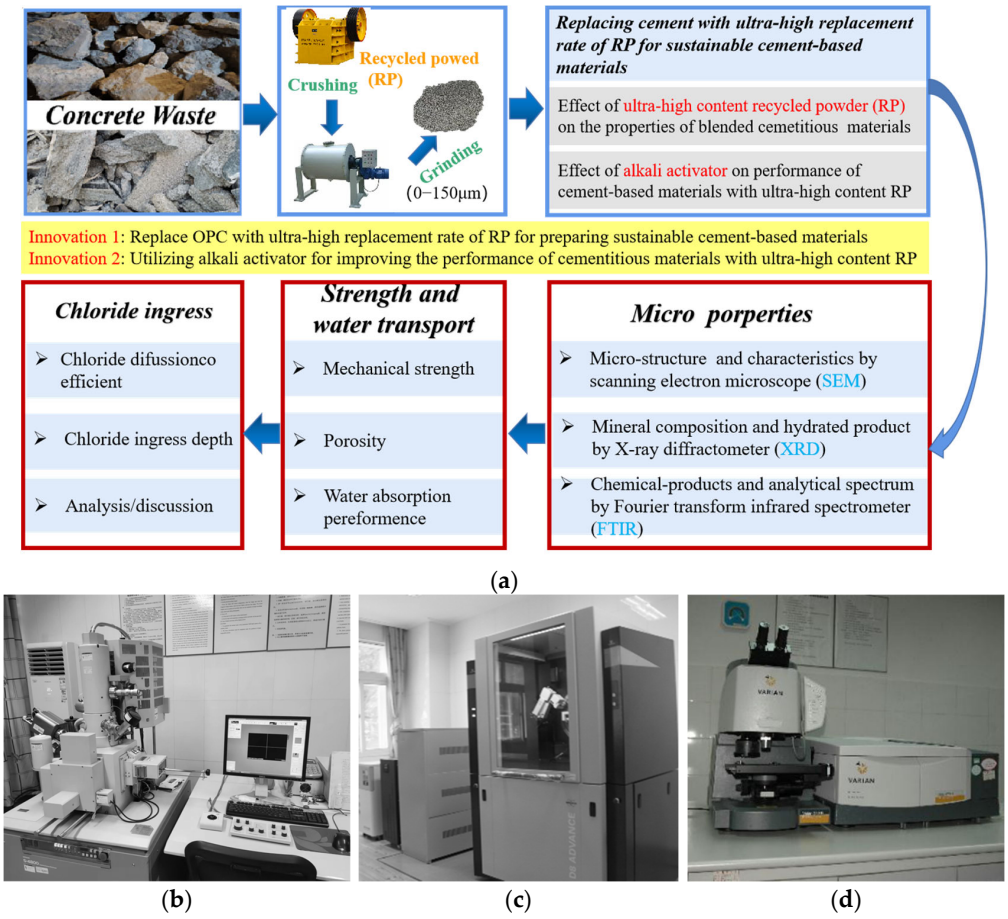

Figure 1. Testing flow of this study and experimental devices: (**a**) experimental process; (**b**) scanning electron microscope (SEM); (**c**) X-ray diffractometer (XRD); (**d**) Fourier transform infrared spectrometer (FTIR).

Table 1 provides the mix proportions for cement-based materials. This study explores the results of alkali activation by using different RP replacement rates and moduli of sodium silicate solutions, with the water-to-binder ratio (W/B) controlled at 0.5 and the binder-to-sand ratio (B/S) set at 1. The solutions were prepared by dissolving analytical-grade sodium hydroxide in distilled water, followed by the addition of sodium silicate solution. "M" following water glass represents the modulus of water glass. By calculating the molar amount of chemicals, the original alkaline content and the required alkaline content for the solution were determined. The alkaline content is expressed as a percentage of the binder. The required amount of water and sodium hydroxide to be added was calculated based on the percentage of solid content of the solution. The modulus of sodium silicate solution used in this experiment was in the range of 1.0 M, 1.2 M, 1.4 M, and 1.6 M, and the alkaline concentration was 6%. Moreover, the experimental sample CBM-70-1.0 M indicated that the sample was prepared using RP to substitute 70% cement, while 1.0 M of water glass was used for alkali activation.

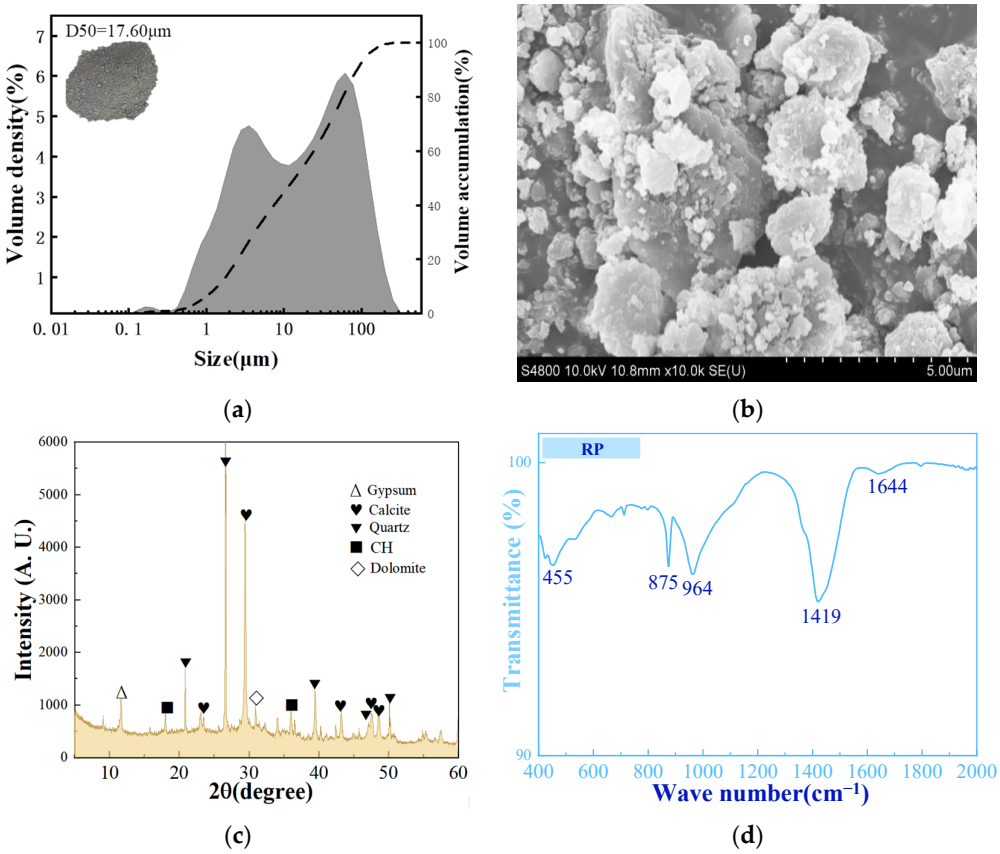

Figure 2. Particle size and components of RP: (**a**) size; (**b**) SEM of RP; (**c**) XRD pattern of RP; (**d**) FTIR of RP.

Table 1. Mix proportions of cement-based material mortar.

Sample	Cement%	RP%	Sodium Silicate	Na%	W/B	B/S
M1	100	0	-	0	0.5	1.0
CBM-70	30	70	-	0	0.5	1.0
CBM-70-1.0	30	70	1.0 M	6	0.5	1.0
CBM-70-1.2	30	70	1.2 M	6	0.5	1.0
CBM-70-1.4	30	70	1.4 M	6	0.5	1.0
CBM-70-1.6	30	70	1.6 M	6	0.5	1.0
CBM-80	20	80	-	0	0.5	1.0
CBM-80-1.0	20	80	1.0 M	6	0.5	1.0
CBM-80-1.2	20	80	1.2 M	6	0.5	1.0
CBM-80-1.4	20	80	1.4 M	6	0.5	1.0
CBM-80-1.6	20	80	1.6 M	6	0.5	1.0
CBM-90	10	90	-	0	0.5	1.0
CBM-90-1.0	10	90	1.0 M	6	0.5	1.0
CBM-90-1.2	10	90	1.2 M	6	0.5	1.0
CBM-90-1.4	10	90	1.4 M	6	0.5	1.0
CBM-90-1.6	10	90	1.6 M	6	0.5	1.0
CBM-100	0	100	-	0	0.5	1.0
CBM-100-1.0	0	100	1.0 M	6	0.5	1.0
CBM-100-1.2	0	100	1.2 M	6	0.5	1.0
CBM-100-1.4	0	100	1.4 M	6	0.5	1.0
CBM-100-1.6	0	100	1.6 M	6	0.5	1.0

In this experiment, a cement mortar mixer was used to first mix OPC and RP at a low speed to ensure uniform blending of the powder. Then, the alkaline activator and sand were added and mixed. The mixture was poured into three molds of different sizes (40 × 40 × 40 mm, 70.7 × 70.7 × 70.7 mm, and the cylinder specimen with the size of 100 mm (diameter) × 50 mm (length)). After 24 h of curing, the mortar was removed from the mold, and the samples were cured in standard conditions for 3 and 28 days.

2.2. Microstructure Determination and Strength

Microscopic structures of the samples were determined by analyzing the microstructure of various cement-based material powders. The SEM was employed to investigate the microstructure of the treated slurry. The materials activated by alkaline were characterized using X-ray diffraction (XRD) analysis. The 2θ range of XRD spectra was 5° to 65°. The porosity of the samples was measured with the vacuum saturation method. Furthermore, the chemical bonds produced by alkaline activation of construction waste were studied using FTIR spectroscopy in the range of 400–2000 cm^{-1}. The position and intensity of the infrared absorption peaks were used to deduce the characteristics of the molecular structure before and after alkaline activation. The specific experimental equipment is shown in Figure 1b,c.

The mechanical properties of cement-based mortar were evaluated by testing the prepared samples (40 × 40 × 40 mm) under different curing times, replacement rates of RP, and alkali-activation moduli. The specimens were subjected to compressive strength testing using a universal testing machine at 3 d, 7 d, and 28 d of curing.

2.3. Water Absorption Curve and Total Porosity

According to the analysis, materials prepared with RP have a relatively high porosity, which affects their durability. To evaluate the water resistance of the materials after the maintenance period, cubic samples (70.7 × 70.7 × 70.7 mm) were vacuum-saturated with water for 24 h. Prior to vacuum saturation, the samples were sealed with molten wax on all sides to allow water to flow in only one direction. The samples were then dried in an oven at 60 °C for 24 h, 48 h, 72 h, and up to 7 days. Mass measurements were taken every 24 h until the difference between the before and after mass did not exceed 0.02%, indicating complete drying. The total porosity of the samples was closely related to the material formation before and after alkali activation. The total porosity was determined by the vacuum saturation method. The total porosity was calculated based on the saturation mass, dry mass, and the mass after drying. Equation (1) shows the detailed calculation method for this method [34], where W_{sat} is the mass of the sample in the surface-dry state, W_{dry} is the mass of the sample in the completely dry state, and W_{wat} is the mass of the sample in water.

$$P = \frac{W_{sat} - W_{dry}}{W_{sat} - W_{wat}} \tag{1}$$

The water absorption rate can be used to verify the relationship between the porosity and the sample. Some researchers [34] have provided relevant calculation formulas to explain this relationship, as indicated by Equation (2):

$$W_a = \frac{m_s - m_d}{m_d} \tag{2}$$

Equation (2) represents the water absorption rate of the sample, where m_s is the mass of the sample at a surface-dry state, and md is the mass of the sample at a completely dry state.

2.4. The Experiment of Rapid Chloride Migration (RCM)

An RCM test was employed to characterize the chloride migration in cement-based materials with ultra-high content of RP in accordance with the Chinese standard [35] and

related references. Equation (3) describes the computational formula of chloride diffusion coefficient (DRCM, 10^{-12} m^2/s):

$$D_{RCM} = \frac{0.0239 \times (273 + T)L}{(U - 2)t}\left(X_d - 0.0238\sqrt{\frac{(273 + T)LX_d}{U - 2}}\right) \quad (3)$$

3. Results

The experimental study involved the use of RP and OPC. Due to the longer curing time and lower strength after hydration, alkali activation was employed. In this study, water glass was used for alkali activation. The hardening of OPC and RP is mostly caused by the gelling substance generated after hydration. Tricalcium silicate generates $Ca(OH)_2$ during hydration, which quickly reaches saturation in water and thus restricts the hydration of both tricalcium and dicalcium silicates. When water glass is mixed with cement slurry, it reacts with the hydration product calcium hydroxide to produce hydrated calcium silicate (C-S-H), which has certain strength. Therefore, the cement–water glass double slurry has higher early strength. The reaction equation is as follows:

$$-Si - O - Si - \overset{OH^-}{\rightarrow} Si - O - + - Si - OH$$

$$-Si - O + OH^- \rightarrow -O - Si - OH$$

$$-Si - O - +Ca^{2+} \rightarrow -Si - O - Ca -$$

$$-Si - O - Ca - +OH^- \rightarrow -Si - O - Ca - OH$$

$$-Si - O - Ca - OH + HO - Si - O \rightarrow -Si - O - Si - +Ca(OH)_2$$

3.1. Results and Discussions on Microscopic Properties

Figure 3 presents the hydration products of cement-based materials with varying replacement rates of different powders. The addition of recycled powder led to the appearance of an obvious steamed bread peak around 20–40°, which corresponds to the formation of C-S-H. The range of the steamed bread peak increases with the increase in the replacement rate of recycled powder, indicating an increase in C-S-H content. At a high replacement rate, the C-S-H and CH provided by RP dominates, while XRD spectra show the output of high content SiO_2 and calcite, mainly derived from natural aggregates in concrete waste. As the hydration products of concrete waste are limited, they mainly provide SiO_2, whereas OPC provides C_2S, C_3S, and CH after hydration. As the replacement rate of RP increases, the number of unreacted quartz and calcite particles also increases [36,37], with absorption peaks at 962 cm^{-1} for Si-O stretching vibration and 1417 cm^{-1} for C-O stretching vibration, indicating the presence of C-S-H and calcite in the reaction products. The results show that the absorption peak at 1646 cm^{-1} does not change significantly after the addition of RP to the cement-based material. The main peak is concentrated at the 962 cm^{-1} Si-O stretching vibration and the 1417 cm^{-1} C-O stretching vibration, indicating that the addition of recycled powder enhances the absorption peaks around 962 cm^{-1} and 1417 cm^{-1}, indicating an increase in calcite and the decrease in C-S-H with the addition of recycled powder.

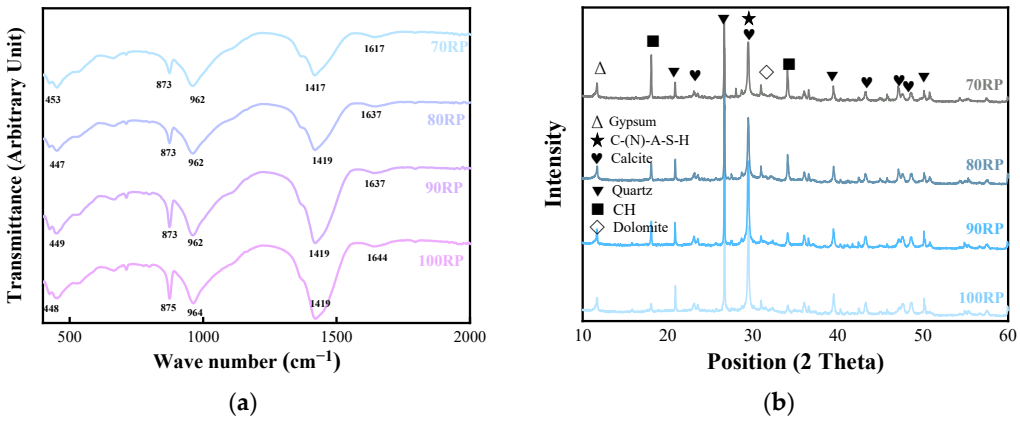

(**a**) (**b**)

Figure 3. XRD pattern and FTIR spectroscopy of different RP replacement rates: (**a**) FTIR spectroscopy of 70–100% RP replacing cement; (**b**) XRD pattern of 70–100% RP replacing cement.

Figure 4 shows the hydration products of cement-based materials with different alkali activator moduli when OPC is partially replaced by 70% RP. The presence of the steamed bread peak at around 20–40° indicates the formation of C-(N)-A-S-H. As the modulus increases, the diffraction angle of the material shifts, indicating a significant increase in the formation of the polymerization products. In addition, RP contains a small amount of active materials and a large amount of inert components such as quartz and calcite. Abundant flocculated C-(N)-A-S-H can be observed, which is due to the increased content of dissolved Al and Si in the material after the addition of concrete waste, which promotes the formation of three-dimensional amorphous aluminosilicate structures [38].

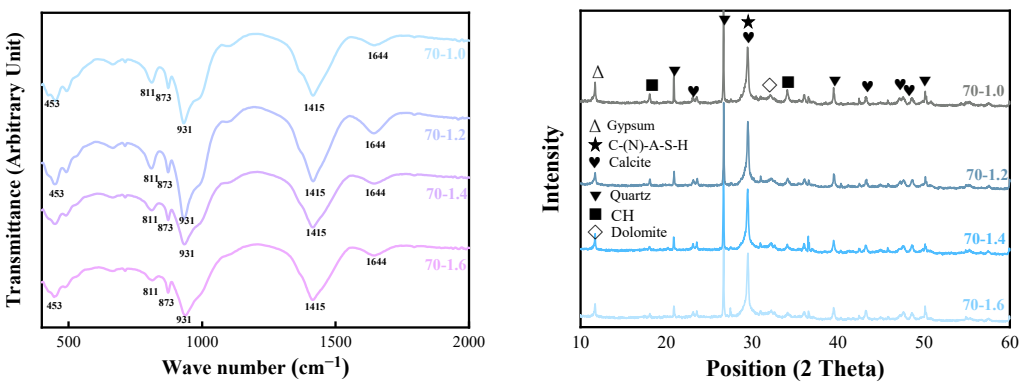

(**a**) (**b**)

Figure 4. XRD pattern and FTIR spectroscopy of different RP replacement rates: (**a**) FTIR spectroscopy of 70% RP replacing cement with 1.0 M, 1.2 M, 1.4 M, and 1.6 M; (**b**) XRD pattern of 70% RP replacing cement with 1.0 M, 1.2 M, 1.4 M, and 1.6 M.

Figure 5 illustrates the effect of different moduli on cement-based materials with a 100% replacement rate, where the recycled powder was added. The appearance of a bread peak around 20–40° is indicative of the polymerization product C-(N)-A-S-H. The range of the peak increases as the modulus of sodium silicate increases, indicating an increase in C-(N)-A-S-H polymerization product. The XRD spectra show a high content of SiO_2 and calcite, as in the stretching vibration of Si-O at 935 cm^{-1}. As the modulus increases, the absorption peak of C-O symmetric stretching vibration decreases. This is mainly due to the low dissolution rate of silicon and aluminum in RP under low-alkali conditions, and the increase in alkali content makes more hydroxide ions come into contact with RP, resulting in a higher dissolution rate of silicon and aluminum. These dissolved ions interact to produce N-A-S-H gel. The results show that when 100%RP replaces cement, the C-O

symmetric stretching vibration of 1417 cm^{-1} obviously decreases with the increase in the modulus of sodium silicate, which is manifested as a decrease in calcite.

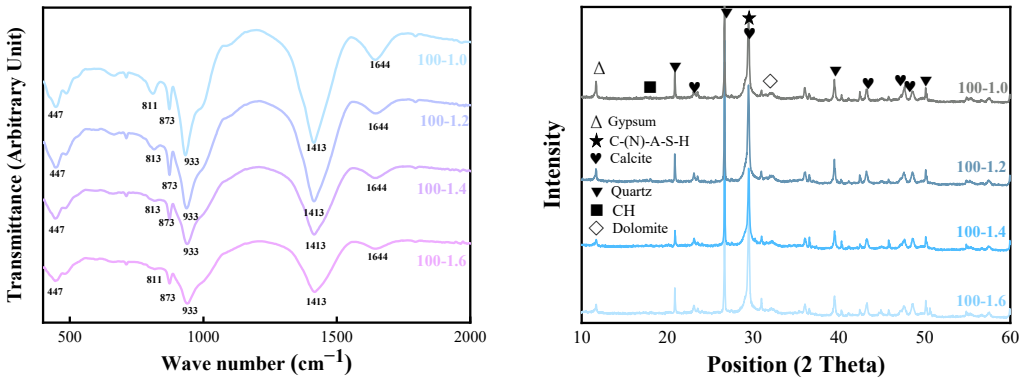

(**a**) (**b**)

Figure 5. XRD pattern and FTIR spectroscopy of 100%RP with alkali activator: (**a**) FTIR spectroscopy of 100% RP replacing cement with 1.0 M, 1.2 M, 1.4 M, and 1.6 M; (**b**) XRD pattern of 100% RP replacing cement with 1.0 M, 1.2 M, 1.4 M, and 1.6 M.

Different microstructures are shown in Figure 6. The results from Figure 6 demonstrate that the control group, which uses Portland cement without any addition of RP, exhibits the most compact structure. When the replacement rate of RP is 70%, the microstructure of the cement-based material is looser, and the SEM images show large blocks of calcium silicate hydrate (C-S-H) with irregular shapes and relatively larger particle sizes, often surrounded by many small particles. When the RP replacement rate is 100%, the microstructure of the material is looser and more cracks can be captured, and there is no good connection between the recycled powder particles and the material. Particles of quartz and calcite, as well as a small portion of C-S-H, are present but poorly connected with the cement-based material. The generated like substance after alkali activation has a good filling effect on the material after alkali activation.

After alkali activation, the structure becomes more compact, as shown in Figure 7, with a portion of hydrated lime and C-S-H formed from the reaction of water glass and hydrated lime. With a constant replacement rate of RP, the content of tricalcium silicate (C_3S) in the cement is constant, and hence the amount of water glass reacting with cement is fixed. As the modulus of water glass increases, more forming substances are produced, leading to a denser structure. After alkali activation, RP particles are enclosed by newly formed polymer products, indicating that the material generated from the water glass activation has a good filling effect on the material. In addition, RP contains a significant amount of inert particles such as quartz and calcite, which dissolve poorly under alkali activation. On the other hand, RP contains a large amount of hydration products such as hydrated calcium silicate and unhydrated cement particles, which easily participate in the new polymerization reaction under alkali activation conditions.

However, the cement-based material with alkali activation and 100% replacement rate has a relatively looser microstructure, as shown in Figure 8. Therefore, using a high content of RP is generally not conducive to the microstructure of the cement-based material slurry [39]. When a high amount of waste powder (100%) is added, there are a large number of particles in the alkali-activated material that are either unreacted or partially reacted, with a poor particle shape, resulting in a looser and porous microstructure. In addition, RP contains a large amount of inert quartz and calcite, which dissolve poorly under alkali activation conditions. Also, RP contains a large number of hydration products (hydrated calcium silicate) and unhydrated cement particles, which are prone to participate in new polymerization reactions under alkali activation conditions. Therefore, the microstructure of the material is relatively dense.

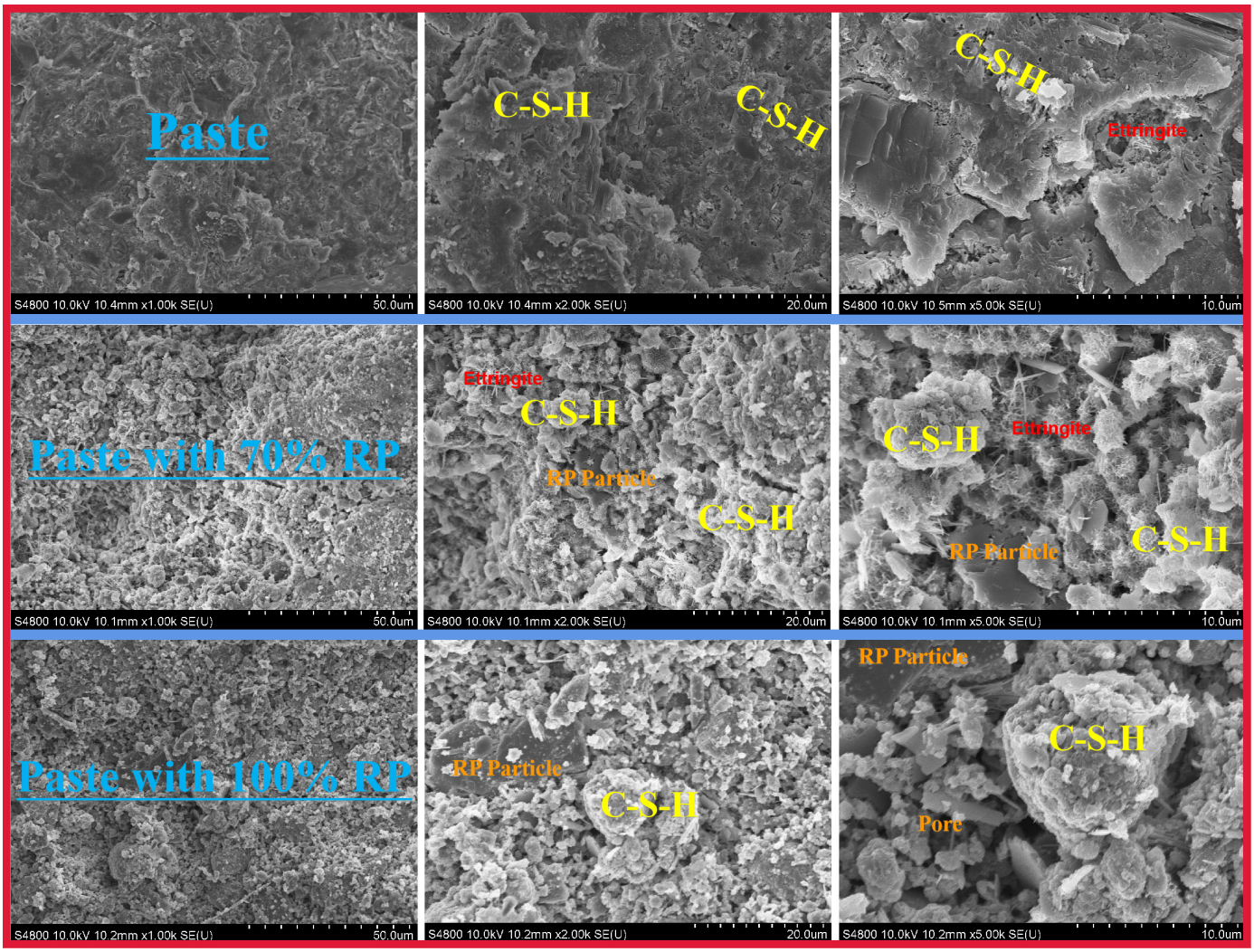

Figure 6. Microstructure and characteristics of different RP replacement rates.

3.2. Results and Discussions on Microscopic Properties

Figure 9 illustrates the mechanical properties of cement-based materials containing construction waste powder under different replacement rates. The compressive strength decreases with an increasing replacement rate of construction waste. The solidification time also decreases with the increase in the replacement rate. The addition of recycled powder results in a decrease in compressive strength of the mixture, but the material still maintains a certain level of strength even at a 100% replacement rate.

CBM-70 exhibited a 76.6% reduction compared to the control group. This is because during the alkali activation process, alkali inhibits cement, and the strength of CBM-80, CBM-90, and CBM-100 decreased by 37.66%, 57.6%, and 99.7%, respectively, compared to CBM-70. As the modulus increased, the mixture exhibited good early strength. For example, CBM-70-1.6 showed an increase of 148% in strength at 3 d compared to CBM-70. CBM-70-1.2 and CBM-70-1.4 also increased by 10.71% and 69.3%, respectively, compared to CBM-70-1.0. At 28 d, CBM-100-1.6 showed an increase in strength of 1297% compared to CBM-100 at a 100% replacement rate, because there were some unreacted cement particles, rich in C-S-H and CH, in the construction waste micro-powders. These active components can be re-aggregated well under alkali activation conditions, leading to the formation of new C-(N)-A-S-H. For example, CBM-100-1.6 showed a strength increase of 629% compared to the unexcited group at 28 d. Although the 28 d compressive strength of the sample decreased significantly after the addition of high-replacement-rate recycled powders, it still

retained a certain level of strength (above 12 MPa). For instance, the strength of CBM-70-1.6, CBM-80-1.6, CBM-90-1.6, and CBM-100-1.6 at 28 d decreased by 34.76%, 42.8%, 48.15%, and 57.58% compared to the control group, but they all exceeded 15 MPa.

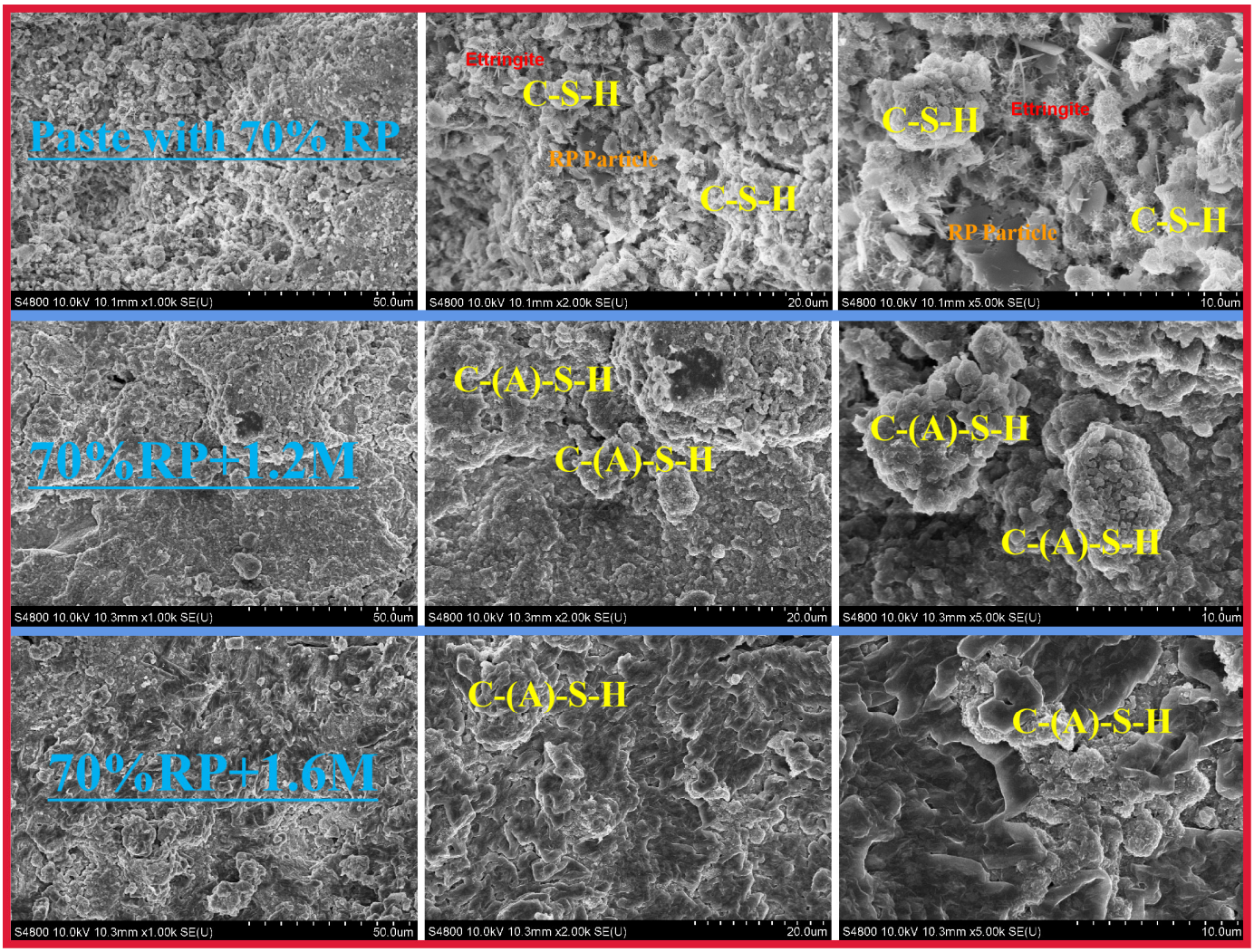

Figure 7. Microstructure and characteristics of 70% RP replacement rate.

As shown in Figure 10, under different concentrations of water glass, with the increase in replacement ratio of recycled powder, the compressive strength of the cement-based material exhibited a decreasing trend. Compared with CBM-70-1.0 and CBM-100-1.0, the strength decreased by 25% and 33% at 3 d and 28 d, respectively. The strength increase of the RP particles in the mortar is derived from the cement hydration product bonding. The addition of excess alkaline substances will inhibit the hydration of cement, leading to a decrease in the strength of RP mortar [40]. As the amount of RP increases, the strength growth of the mortar is due to both the cement hydration product bonding with RP and the activation of the reactive materials of RP. This activation reaction consumes the alkaline substance and reduces the system's alkalinity, which weakens the inhibition of cement hydration and promotes the hydration degree, thus increasing the compressive strength of the sample.

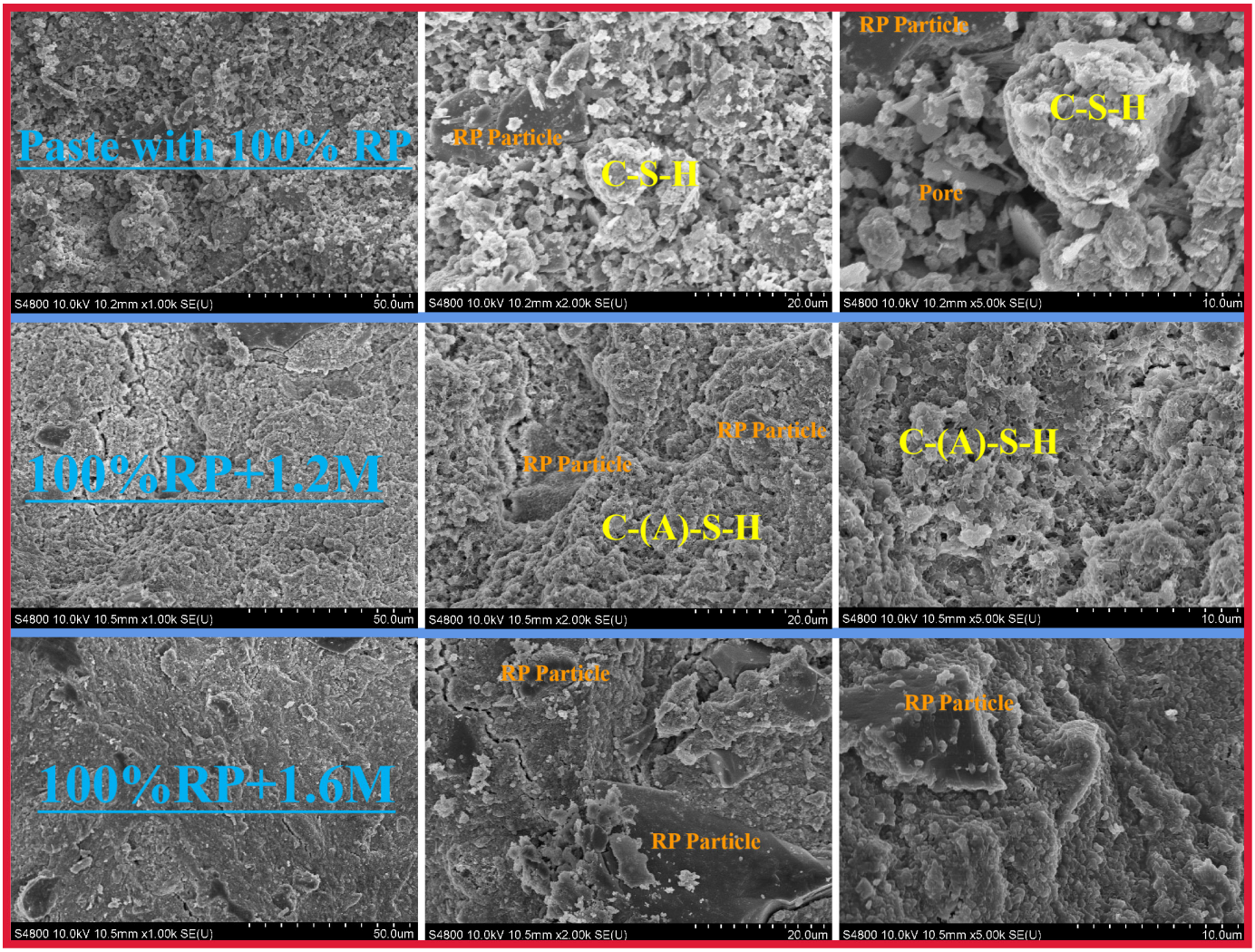

Figure 8. Microstructure and characteristics of 100% RP replacement rate.

At the 1.2 and 1.4 moduli, under the 80% replacement rate, the compressive strength at 3 days showed a slight increase compared with the 70% replacement rate. Meanwhile, the strength of CBM-70-1.2 and CBM-100-1.2 only decreased by 10.5% at 3 days, and the strength of CBM-70-1.4 and CBM-100-1.4 decreased by 16.5%. This may be due to the fact that the main components of construction waste fine powder are inert SiO_2 and $CaCO_3$, which act as non-reactive fillers in the alkaline activation reaction and are difficult to activate, resulting in a decrease in strength. RP in the cement-based system, as the main cementing material, may have a negative effect on strength development because it contains a large amount of calcium [41]. The addition of RP can slow down the dissolution process of alkali-activated materials because the surface may be enveloped by calcium-rich products [42].

With an increase in the water glass modulus, the curing time decreased, and the compressive strength of CBM-70-1.0 was only around 8 MPa, while it was approximately 6 MPa for the 100% replacement. When activating the sample using an activator with a modulus of 1.2, its strength was the same as that of CBM-70-1.0 after three days of curing. The 28-day strength of CBM-70-1.0 was about 12 MPa, while the strength of CBM-100-1.6 increased by 6.3% after three days, indicating that the use of high-modulus alkali activation promotes early strength development to some extent. This is because the addition of 100% RP compensates for the strength of cement-based material through a small amount of hydrated C-S-H and CH in RP, and then participates in new alkali activation reactions,

thus promoting the development of compressive strength. Furthermore, under a fixed replacement rate, a comparison of the results of alkali activators with different moduli shows that the compressive strength of high-modulus activators is higher than that of low-modulus activators, and the difference in compressive strength is more significant when a large amount of construction waste powder is added. For example, the 28-day compressive strength of CBM-100-1.6 increases by 44.25%, 38.3%, and 1.02% compared to CBM-70-1.0, CBM-70-1.2, and CBM-70-1.4, respectively. This figure establishes the relationship between the replacement rate of construction waste powder and the mechanical properties of the prepared mixture. With the increase in the replacement rate, the mechanical properties decreased linearly.

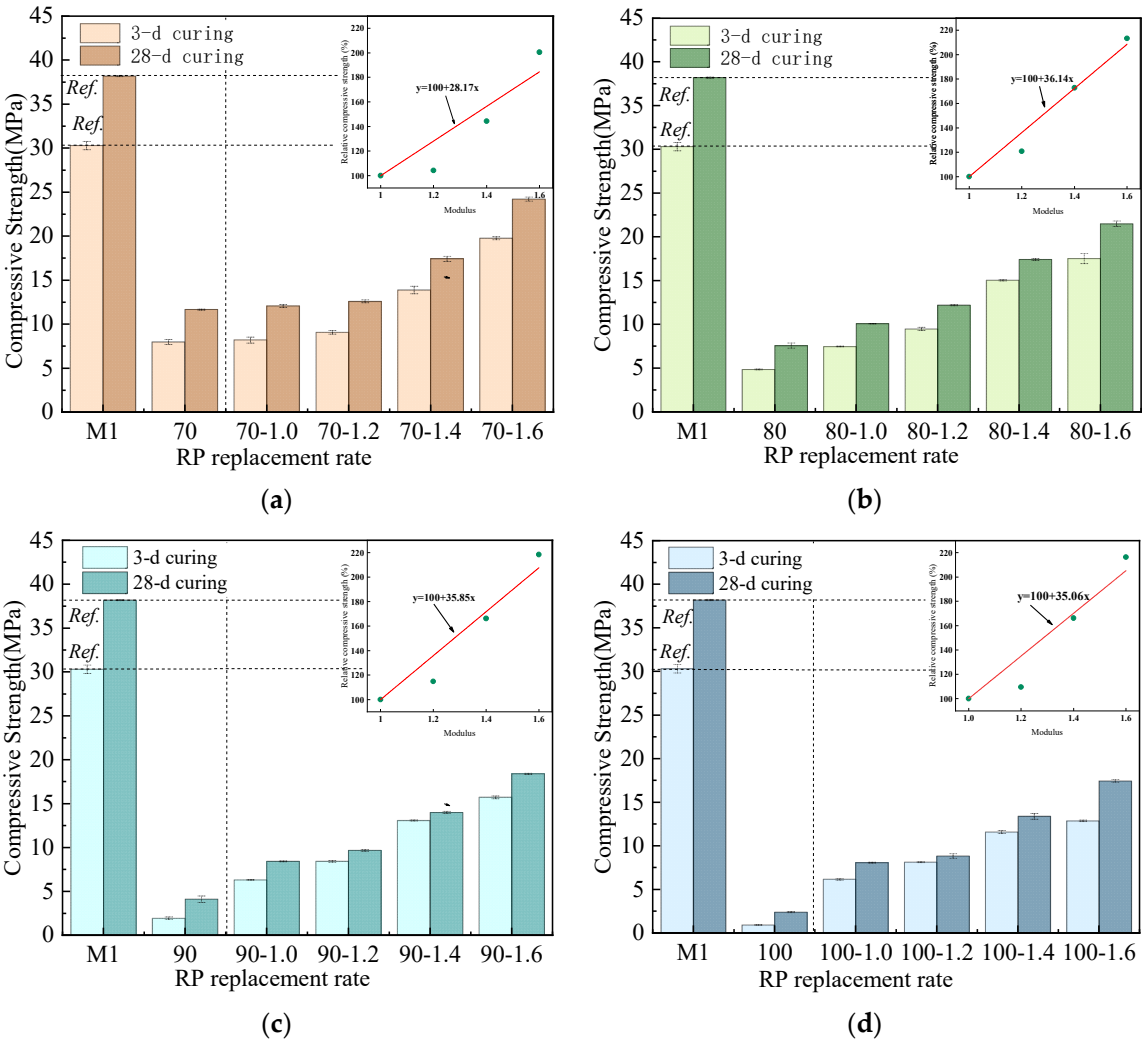

Figure 9. Compressive strength with different RP replacement rates: (**a**) 70% RP replacing cement; (**b**) 80% RP replacing cement; (**c**) 90% RP replacing cement; (**d**) 100% RP replacing cement.

3.3. The Analysis of Water Absorption Curve and Total Porosity

When the replacement rate of recycled powder (RP) was 100%, the water absorption of the cement-based mortar with 100%RP was slightly higher than that of the cement-based mortar without RP. This is because using RP as a replacement for 100% ordinary Portland cement (OPC) leads to a looser and porous microstructure, which causes rapid water absorption in the RP-based mortar due to cracks and pores. After alkali activation, the water absorption rate slightly increased due to the pore formation caused by the aggregation of the generated hydrated calcium silicate substance after alkali activation modification.

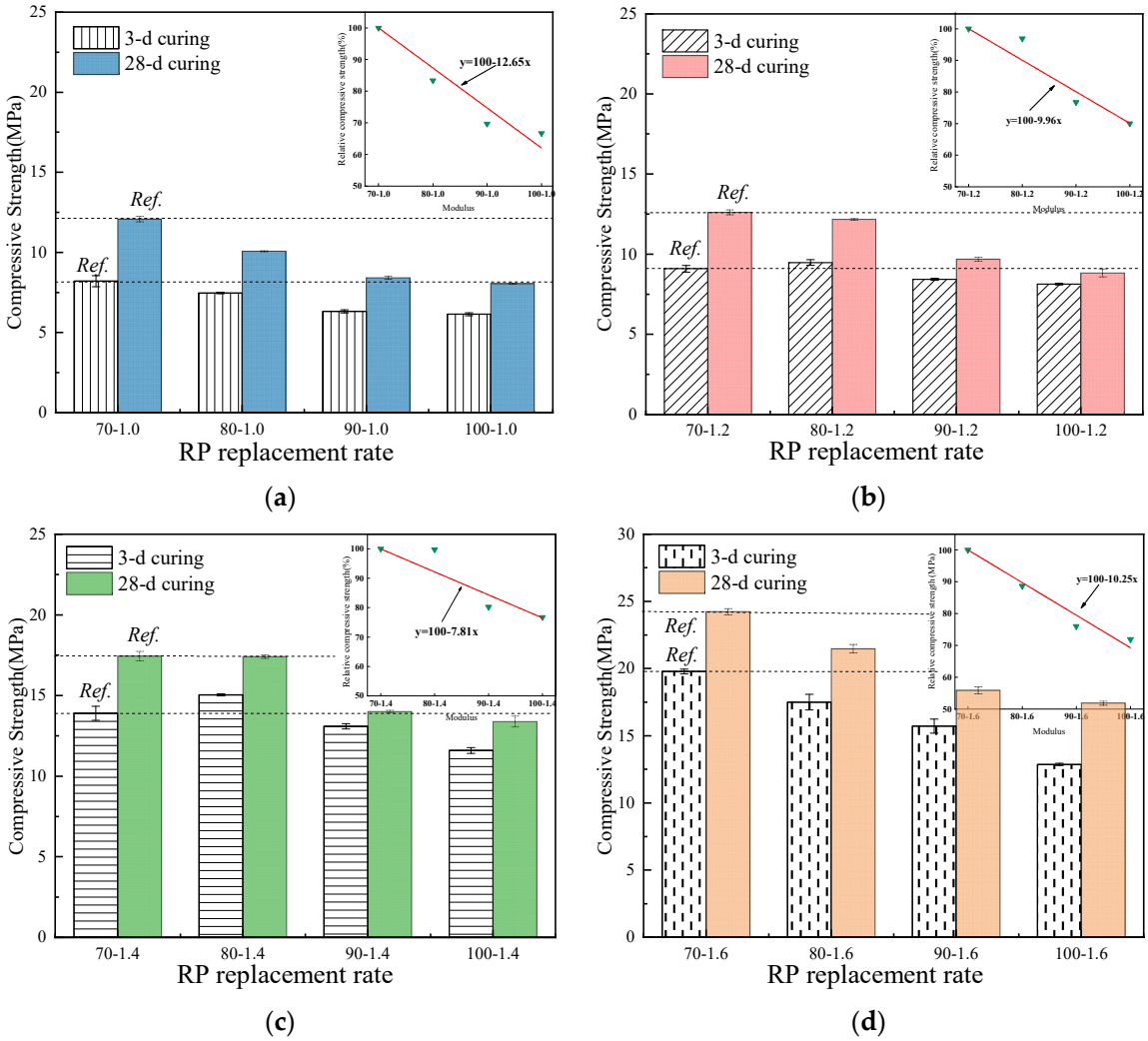

Figure 10. Compressive strength with different modulus of water glass: (**a**) 1.0 modulus; (**b**) modulus; (**c**) 1.4 modulus; (**d**) 1.6 modulus.

Figure 11 shows the transport properties of the cement-based material to characterize its durability, and the effect of the modulus of alkali activation on the water absorption rate of mortar with different replacement ratios of recycled powder. It can be seen that as the modulus increased, the water absorption rate increased slightly. However, at a replacement rate of 70%, the water absorption rate of CBM-70 cement-based mortar with recycled powder was similar to that of CBM-70-1.6 cement-based mortar, while the water absorption rates of CBM-70-1.2, CBM-70-1.4, and CBM-70-1.6 were increased by 1.19%, 2.39%, and 2.43%, respectively, compared to that of CBM-70-1.0. The incorporation of recycled powder increased the content of inert components, leading to a reduction in C-(A)-S-H, and the newly formed pores provided channels for water penetration in the material. At the replacement rate of 100%, the water absorption rate of CBM-100 cement-based mortar was reduced by 1.83% compared to that of CBM-100-1.6 cement-based mortar. Meanwhile, the water absorption rate of CBM-80-1.6 was increased by 2.44% compared to that of CBM-80-1.0, and the water absorption rate of CBM-90-1.6 was increased by 1.62% compared to that of CBM-90-1.0. The water absorption rate of CBM-100-1.6 was increased by 1.74% compared to that of CBM-100-1.0. It can be observed that although the water absorption rate shows an upward trend with the increase in the modulus under alkali activation conditions, the water absorption rates of cement-based mortar with a modulus of 1.0 and 1.6 are basically the same.

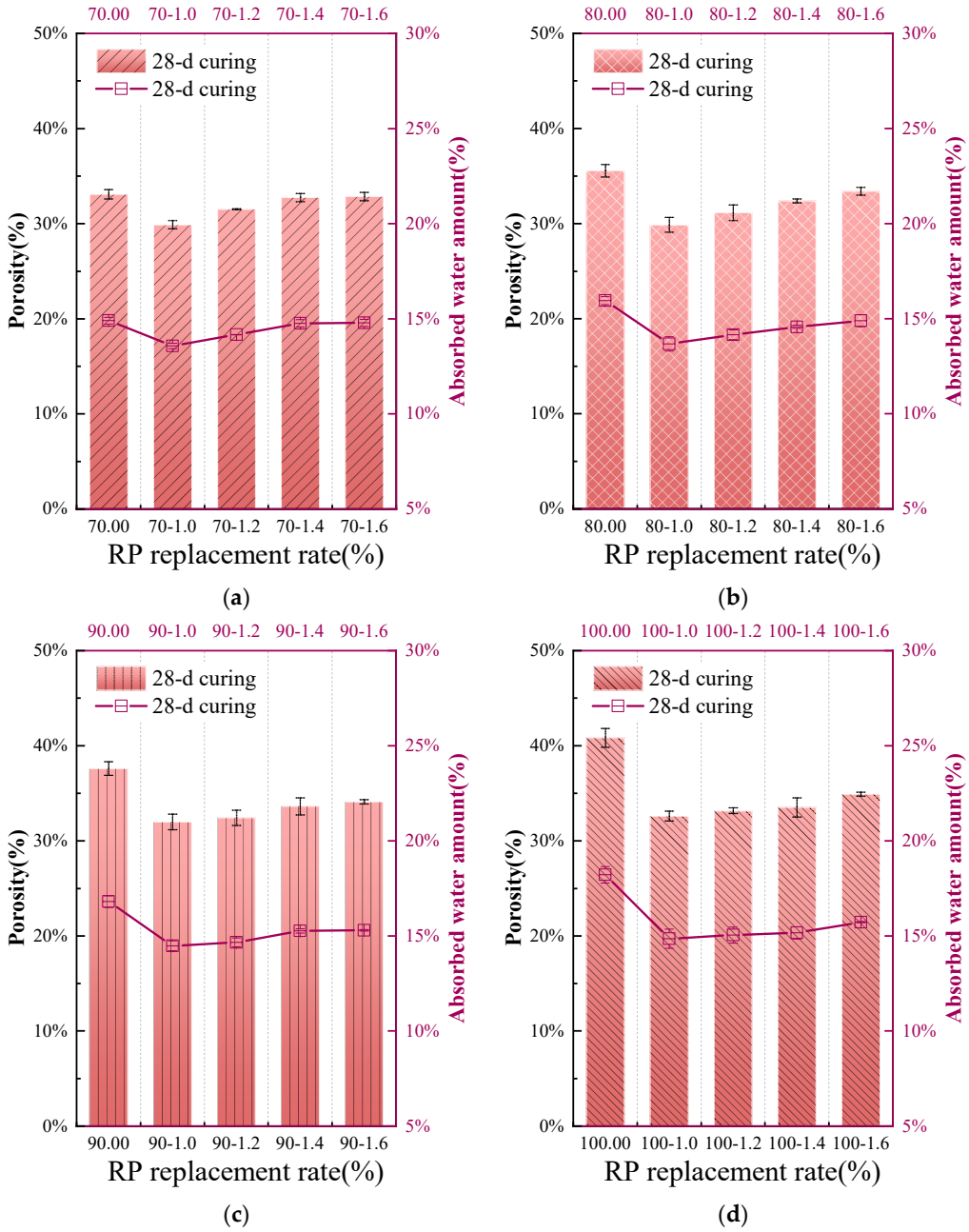

Figure 11. Water absorption curves and total porosity with different RP rates: (**a**) 70% RP replacing cement; (**b**) 80% RP replacing cement; (**c**) 90% RP replacing cement; (**d**) 100% RP replacing cement.

The water absorption of cement-based mortar without alkaline activation is significantly higher than that of mortar with alkaline activation. This effect was particularly pronounced when the replacement rate of cement reached 100%. CBM-70 increased by 2.67% compared to CBM-70-1.0, CBM-80 increased by 4.54% compared to CBM-80-1.0, CBM-90 increased by 4.64% compared to CBM-90-1.0, and CBM-100 increased by 6.72% compared to CBM-100-1.0. As the amount of RP increased, the water absorption also increased slightly. This is because replacing cement with RP produces a looser and porous microstructure, which causes rapid water absorption of the cement-based mortar. When the replacement rate reached 100%, the porosity reached its maximum. With an increase in the alkaline activator modulus, the porosity also increased. Conversely, the compressive strength increased with a decrease in micro-porosity and average pore size, indicating a denser internal structure. Under the condition of a fixed modulus of water glass, as the

amount of RP increased, the porosity of the mortar increased and the average pore size also increased, which is opposite to the change trend of the compressive strength.

Meanwhile, Figure 11 illustrates the influence of different modulus on the total porosity of cement-based mortars. The total porosity of RP-containing cement-based mortars after alkali activation increased with the increase in the modulus of water glass. Under the same curing time, the total porosity of cement-based mortars activated with a modulus of 1.6 was similar to that of the unactivated material with a 70% replacement rate, and the total porosity of cement-based mortars with the moduli of 1.2, 1.4, and 1.6 was slightly higher than that of cement-based mortars with 1.0 modulus. The total porosity of CBM-70-1.0, CBM-70-1.2, CBM-70-1.4, and CBM-70-1.6 was 29.9%, 31.53%, 32.76%, and 32.88%, respectively, but all were lower than the unactivated control group at the same replacement rate. This trend was observed as the replacement rate increased. CBM-80-1.6, CBM-90-1.6, and CBM-100-1.6 had total porosities that were 2.16%, 3.49%, and 3.49% higher than their respective unactivated control groups.

Figure 12 illustrates the effect of different replacement levels on the water absorption of materials at the same molarity. It can be observed that the water absorption increased with the increase in replacement level, but the overall increase was not significant when it reached 100% replacement level. CBM-100-1.0 had a 2.43% higher water absorption rate compared to CBM-70-1.0, while CBM-100-1.2 had a 2.44% higher rate compared to CBM-70-1.2. Similarly, CBM-100-1.4 and CBM-100-1.6 had increases of 1.62% and 1.74%, respectively, compared to CBM-70-1.4 and CBM-70-1.6. The microstructure of both the polymerization activity and the recycled powder affected the water absorption performance of cement-based materials. Specifically, the RP contains a large number of porous microstructures of calcium silicate hydrate. When the replacement level of RP was 100%, the water absorption rate of the 100% recycled powder material mortar was significantly higher than that of other replacement levels.

Furthermore, Figure 12 also displays the total porosity of cement-based mortars containing different RP replacement rates. The total porosity of the cement-based mortar containing RP increased with the increase in RP replacement rate. When the curing times were the same, the total porosity of the cement-based mortar containing 70% RP was similar to that of the cement-based mortar using 1.6 modulus water glass. The total porosity of the cement-based mortar with RP replacement levels of 80%, 90%, and 100% was slightly higher than that of the cement-based mortar with a 70% replacement level. For instance, CBM-80, CBM-90, and CBM-100 had total porosity levels of 35.58%, 37.61%, and 40.84%, respectively. The results show that the addition of recycled powder leads to a significantly higher porosity compared to the cement-based reference group. Specifically, CBM-70, CBM-80, CBM-90, and CBM-100 had 14.65%, 17.12%, 19.15%, and 22.38% higher total porosity than the M1.

As shown in Figure 13e, the chloride diffusion coefficient of the mixture increased with the increase in RP replacement rate. For example, CBM-70, CBM-80, CBM-90, and CBM-100 increased by 84.6%, 93.4%, 142.8%, and 160.7%, respectively, compared with the cement control group. However, the addition of alkali activators can reduce chloride diffusion. Compared with CBM without alkali activation, CBM-70-1.2, CBM-80-1.2, CBM-90-1.2, and CBM-100-1.2 reduced the penetration by 18.3%, 14.9%, 29.8%, and 25.9%, respectively. In addition, Figure 13a–d show the chloride diffusion depth of cement-based materials after alkali activation. With the increase in the sodium silicate modulus, the chloride intrusion depth decreased. The addition of alkali-activated C-(N)-S-H refined the pore structure of cement-based material due to its high alkali activation activity. Under the condition of an RP replacement rate of 70%, CBM-70-1.2 and CBM-70-1.6 reduced the chloride penetration depth by 18.3% and 24.1%, respectively, compared with the cement control group with an RP replacement rate of 70%. When the replacement rate reached 100%, CBM-100-1.2 and CBM-100-1.6 reduced the penetration depth by 25.9% and 35.1%, respectively, compared with CBM-100 without alkali activation.

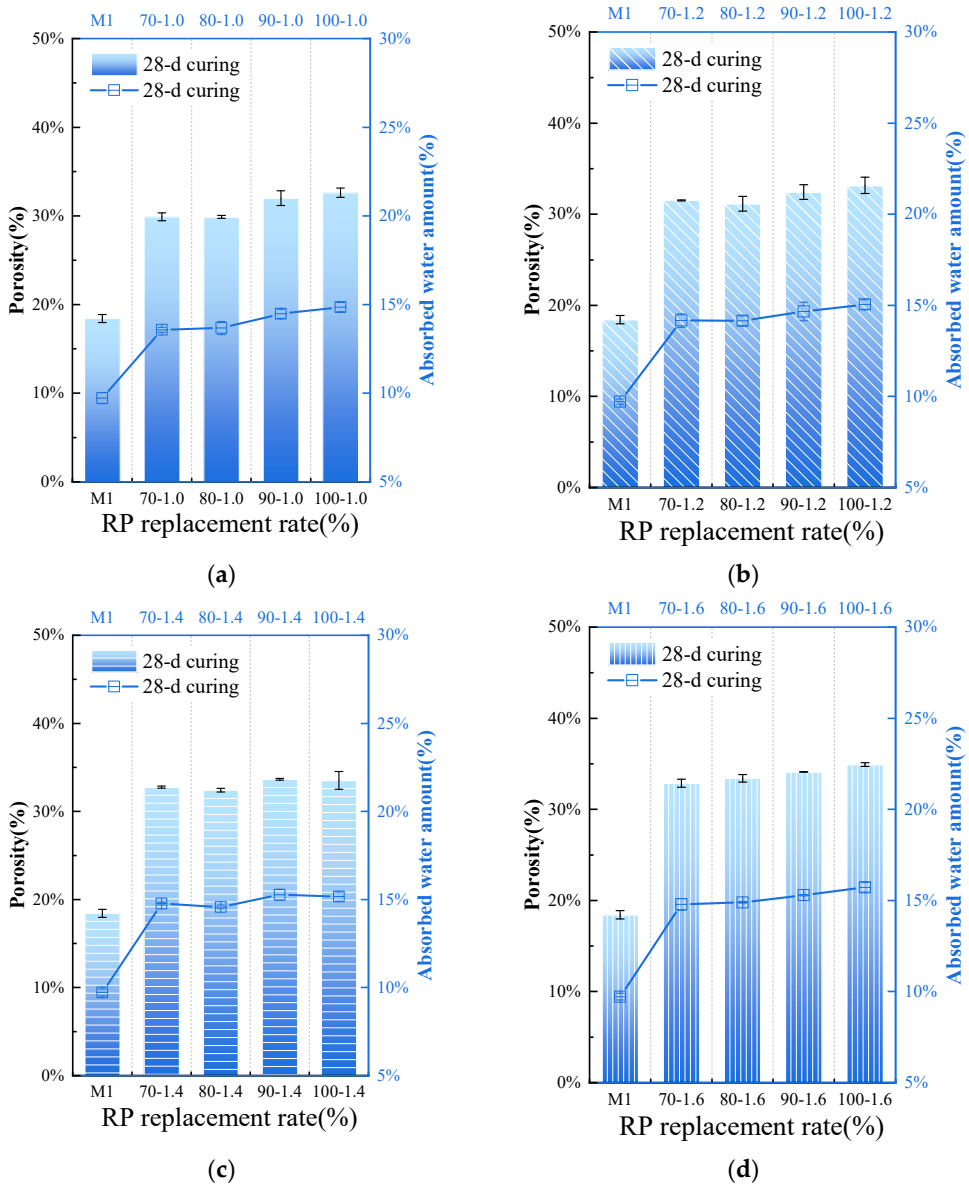

Figure 12. Water absorption curves and total porosity with different moduli: (**a**) 1.0 modulus; (**b**) modulus; (**c**) 1.4 modulus; (**d**) 1.6 modulus.

3.4. Economic and Environmental Benefits Evaluation

The production of cement results in high energy consumption, significant CO_2 emissions, and costs. However, the preparation of RP offers lower CO_2 emissions and costs compared to cement preparation. Moreover, the use of alkali-activated RP mortar provides better economic and environmental benefits. Therefore, by utilizing an appropriate sodium silicate solution for activating cement mortar, it is possible to reduce CO_2 emissions and achieve economic benefits. Tables 2 and 3 present the calculation of unit costs and carbon footprints for alkali-activated mixing, based on previous research literature references [43–49]. Using an excitation ratio of 100-1.6 M, a 67.9% reduction in CO_2 emissions and a 19.55% reduction in cost per MPa can be achieved. These findings highlight the environmental and economic advantages of using RP in cement-based materials.

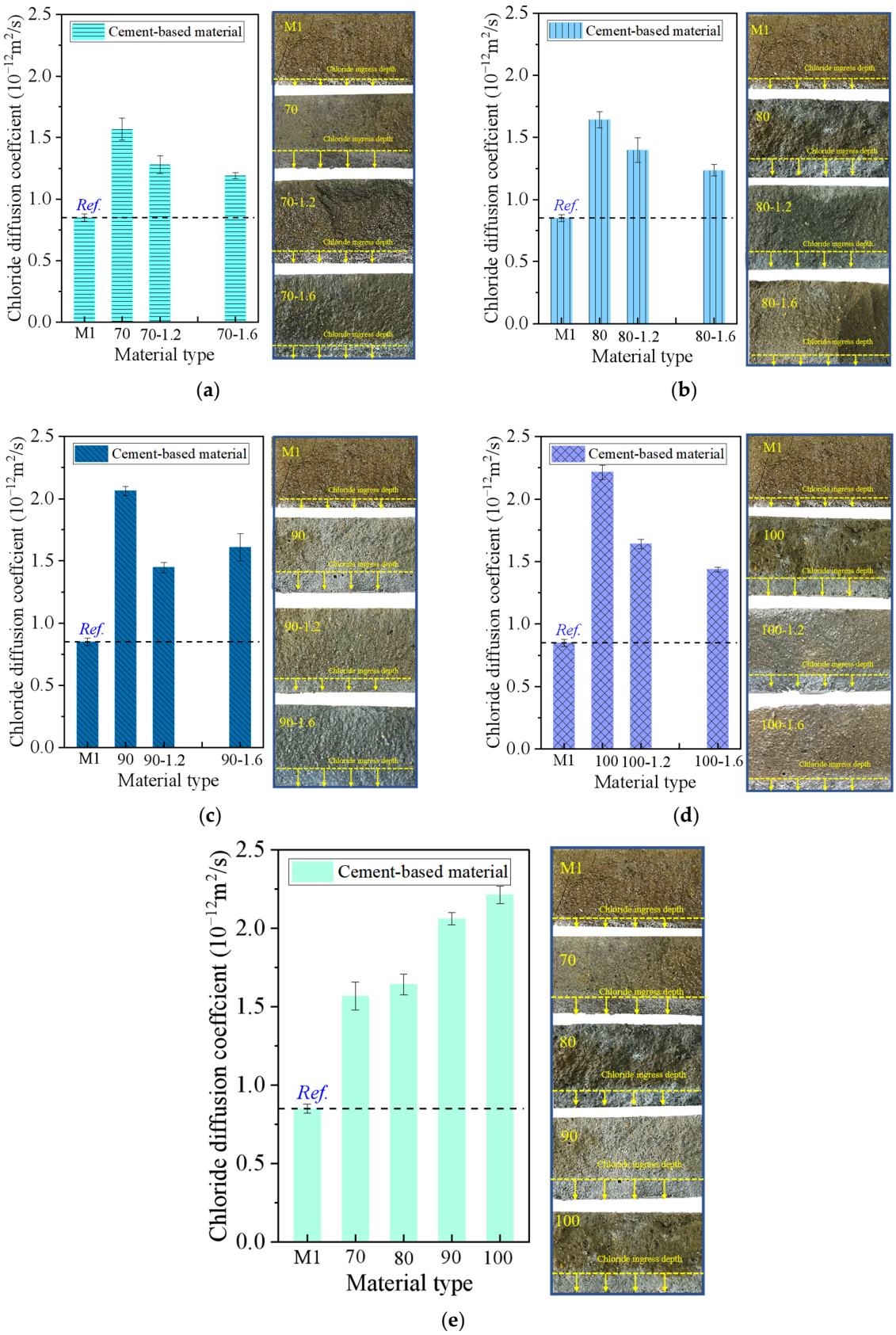

Figure 13. Chloride ingress into cement-based material incorporated with different RP rates and alkali excitation moduli: (**a**) 70% RP; (**b**) 80% RP; (**c**) 90% RP; (**d**) 100% RP; (**e**) different RP rate.

Table 2. CO_2 emissions per cubic meter.

Materials	CO_2 Emission (kg)	CO_2 Emission				
		Cement	70-1.6 M	80-1.6 M	90-1.6 M	100-1.6 M
Cement	0.82 [43]	984	295.2	196.8	98.4	0
RP	0.004 [44]	/	3.36	3.84	4.32	4.8
Na_2SiO_3	0.78 [45]	/	37.44	37.44	37.44	37.44
NaOH	1.425 [45]	/	272.95	272.95	272.95	272.95
Water	/	/	/	/	/	/
Total emission	/	984	608.95	511.03	413.11	315.19

Table 3. Cost per cubic meter.

Materials	Cost (USD/kg)	Cost				
		Cement	70-1.6 M	80-1.6 M	90-1.6 M	100-1.6 M
Cement	0.32 [44]	416	115.2	76.8	38.4	0
RP	0.021–0.064 [46,47]	/	53.76	61.44	69.12	76.8
Na_2SiO_3	1.00 [48]	/	58.28	58.28	58.28	58.28
NaOH	0.37 [49]	/	17.76	17.76	17.76	17.76
Water	/	/	/	/	/	/
Total emission	/	416	245	214.28	183.56	152.84
C(cost/MPa)	/	10.89	10.11	9.97	9.98	8.76

3.5. Discussions and Suggestions

Previous investigations have confirmed the feasibility of utilizing RP as an alternative binder in sustainable cement-based materials. However, the effects of ultra-high RP replacement on the properties of blended cement-based materials have received limited attention in the relevant literature. Studies have also reported that the addition of RP has a detrimental impact on the micro–macro properties of blended cement-based materials, with a significant reduction in properties observed when RP replacement rates reach 30–50% [50–52]. Specifically, Wu et al. [51] reported a 27.2% and 43.7% reduction in the compressive strength of mortar when using 30% and 50% RP as a cement replacement, respectively. Therefore, it is suggested that the RP replacement rate in cement-based materials should be kept below 30% unless effective modification methods are employed [8]. The findings of this study further clarify the effects of ultra-high RP replacement ratios on the micro–macro properties of cement-based materials. The results demonstrate that the incorporation of ultra-high replacement levels (70–100%) of RP significantly adversely affects the microstructural and macroscopic properties of cement-based materials.

As a result, mortar and concrete containing ultra-high contents of RP are not recommended for use in construction engineering due to their inferior properties. Furthermore, traditional modification methods, such as mechanical strength enhancement and nano-modification, are ineffective in improving the properties of cement-based materials with ultra-high RP content [8,53]. This study provides an effective approach to enhancing the microstructure and macro properties of cement-based materials containing ultra-high RP content through the addition of alkali activators. Several significant and encouraging conclusions have been drawn. By optimizing the content of RP, cement, and alkali activators, it is possible to achieve cement-based materials with ultra-high RP content that exhibit good microstructure, strength, and durability performance. Additionally, the utilization of ultra-high RP content in cement-based materials can rapidly reduce the amount of construction and demolition waste and diminish the need for cement in construction engineering, contributing to environmental sustainability.

4. Conclusions

This article investigates the microstructure and macroscopic properties of cement-based materials prepared from construction waste under alkali activation conditions. Based on the research findings and discussions, the following conclusions can be drawn.

(1) The construction waste and its preparing RP also contains some hydration products and inert substances such as quartz and calcite, and the large-volume incorporation of RP reduces the polymerization reaction of the newly prepared materials. When RP is used instead of 100% cement to prepare cement-based materials, the pore structure increases and the microstructure becomes loose.
(2) With the increase in RP substitution rate, the mechanical strength of cement-based materials generally decreases, while the water absorption and total porosity increase significantly. The 3 d strength of CBM-70, CBM-80, CBM-90, and CBM-100 decreased by 73.63%, 84.06% and 93.65%, and 96.98%, respectively, compared with the pure cement control group. The 3 d strength of CBM-100 was only 0.89 MPa. The 28 d intensities of the control group were 30.54%, 19.82%, 10.79%, and 6.26%, respectively.
(3) Alkali excitation of cement-based materials with water glass solution can optimize the performance of a large-volume RP mixture. Under the action of 1.0 M activator, the 3 d strength of 70%, 80%, 90%, and 100%RP mortar increased by 2.71%, 13.63%, 73.86%, and 147.31% compared with that without excitation. After 28 d of maintenance, the strength increased to 3.6%, 8.05%, 49.5%, and 107.71%.
(4) Changing the modulus and concentration of the alkali activator can improve the performance of cement-based materials under a high substitution rate, so as to obtain materials with good mechanical strength and durability. With the increase in water glass modulus, its mechanical properties also showed an increasing trend. At 70%RP substitution rate, the strength of 1.0 M, 1.2 M, 1.4 M, and 1.6 M regenerated micro-powder mortar increased by 3.6%, 8.05%, 49.5%, and 107.71% compared with that of unexcited mortar. When the RP replacement rate was 100%, the strength of 1.0 M, 1.2 M, 1.4 M, and 1.6 M reclaimed micro-powder mortar was 8.06 MPa, 8.83 MPa, 13.39 MPa, and 17.44 MPa, respectively.
(5) With the increase in construction waste substitution rate, the diffusion coefficient of chloride ions increases, and the immersion depth of chloride ions increases. CBM-70, CBM-80, CBM-90, and CBM-100 were, respectively, 71.9%, 79.3%, 121.3%, and 136.5% higher than the cement reference group. After alkali excitation, the diffusion coefficient and penetration depth of chloride ions of cement-based materials are reduced, and the chloride ion penetration can be further reduced by increasing the modulus of water glass. CBM-100-1.2 and CBM-100-1.6 were 25.9% and 35.1% lower than CBM-100.

Author Contributions: Methodology, Y.Z.; formal analysis, Z.Z.; investigation, R.H. and Y.Z.; data curation, Z.Z.; writing—original draft, R.H.; writing—review & editing, Y.Z.; visualization, Z.Z.; supervision, Z.M.; project administration, Z.M.; funding acquisition, Z.M. All authors have read and agreed to the published version of the manuscript.

Funding: This research was funded by the Natural Science Foundation of Jiangsu Province, grant number BK20200957.

Institutional Review Board Statement: Not applicable.

Informed Consent Statement: Not applicable.

Data Availability Statement: Not applicable.

Conflicts of Interest: The authors declare no conflict of interest in this research.

References

1. Kurda, R.; Brito, J.D.; Silvestre, J.D. A comparative study of the mechanical and life cycle assessment of high-content fly ash and recycled aggregates concrete. *J. Build. Eng.* **2022**, *29*, 101173. [CrossRef]
2. Jike, N.; Xu, C.; Yang, R.; Qi, Y. Pervious concrete with secondarily recycled low-quality brick-concrete demolition residue: Engineering performances, multi-scale/phase structure and sustainability. *J. Clean. Prod.* **2022**, *341*, 130929. [CrossRef]
3. Basaran, B.; Kalkan, I.; Aksoylu, C.; Özkılıç, Y.O.; Sabri, M.M.S. Effects of waste powder, fine and coarse marble aggregates on concrete compressive strength. *Sustainability* **2022**, *14*, 14388. [CrossRef]
4. Ren, P.; Li, B.; Yu, J.; Ling, T.C. Utilization of recycled concrete fines and powders to produce alkali-activated slag concrete blocks. *J. Clean. Prod.* **2020**, *267*, 122115. [CrossRef]
5. Vintimilla, C.; Etxeberria, M.; Li, Z. Durable Structural Concrete Produced with Coarse and Fine Recycled Aggregates Using Different Cement Types. *Sustainability* **2023**, *15*, 14272. [CrossRef]
6. Wang, Y.; Lu, Z.; Wang, D.; Tan, Q.; Wu, W.; Zhu, L. Influence of Recycled Cement Paste Powder on Early-Age Plastic Shrinkage and Cracking of Cement-Based Materials. *Sustainability* **2023**, *15*, 10661. [CrossRef]
7. Lin, Y.; Maghool, F.; Arulrajah, A.; Horpibulsuk, S. Alkali activation of recycled concrete and aluminum salt slag aggregates for semi-rigid column inclusions. *Constr. Build. Mater.* **2023**, *366*, 130106. [CrossRef]
8. Tang, Q.; Ma, Z.; Wu, H.; Wang, W. The utilization of eco-friendly recycled powder from concrete and brick waste in new concrete: A critical review. *Cem. Concr. Compos.* **2020**, *114*, 103807. [CrossRef]
9. Wu, H.; Hu, R.; Yang, D.; Ma, Z. Micro-macro characterizations of mortar containing construction waste fines as replacement of cement and sand: A comparative study. *Constr. Build. Mater* **2023**, *383*, 131328. [CrossRef]
10. Boudali, S.; Abdulsalam, B.; Rafiean, A.H.; Poncet, S.; Soliman, A.; ElSafty, A. Influence of fine recycled concrete powder on the compressive strength of selfcompacting concrete (SCC) using artificial neural network. *Sustainability* **2021**, *13*, 3111. [CrossRef]
11. Bao, J.; Li, S.; Yu, Z.; Xu, J.; Li, Y.; Zhang, P.; Si, Z.; Gao, S. Water transport in recycled aggregate concrete under sustained compressive loading: Experimental investigation and mesoscale numerical modelling. *J. Build. Mater.* **2021**, *44*, 103373. [CrossRef]
12. Ma, Z.; Shen, J.; Wang, C.; Wu, H. Characterization of sustainable mortar containing high-quality recycled manufactured sand crushed from recycled coarse aggregate. *Cem. Concr. Compos.* **2022**, *132*, 104629. [CrossRef]
13. Hamdadou, M.; Bignonnet, F.; Deboucha, W.; Ranaivomanana, H.; Leklou, N.; Arroudj, K. Hydration, mechanical and transfer properties of blended cement pastes and mortars prepared with recycled powder or limestone filler. *J. Build. Eng.* **2023**, *78*, 107541. [CrossRef]
14. Jx, A.; Zm, A.; Tx, B.; Aa, C.; Zd, A. Mechanical properties of concrete mixed with recycled powder produced from construction and demolition waste. *J. Clean. Prod.* **2018**, *188*, 720–731.
15. Li, C.; Li, J.; Ren, Q.; Zheng, Q.; Jiang, Z. Durability of concrete coupled with life cycle assessment: Review and perspective. *Cem. Concr. Compos.* **2023**, *139*, 105041. [CrossRef]
16. Horsakulthai, V. Effect of recycled concrete powder on strength, electrical resistivity, and water absorption of self-compacting mortars. *Case Stud. Constr. Mater.* **2021**, *15*, e00725. [CrossRef]
17. Mehdizadeh, H.; Ling, T.C.; Cheng, X.; Mo, K.H. Effect of particle size and CO_2 treatment of waste cement powder on properties of cement paste. *Can. J. Civ. Eng.* **2021**, *48*, 522–531. [CrossRef]
18. Fernandes, B.; Carré, H.; Mindeguia, J.; Perlot, C.; La, B. Effect of elevated temperatures on concrete made with recycled concrete aggregates-An overview. *J. Build. Eng.* **2021**, *44*, 103235. [CrossRef]
19. Xu, L.; Wang, J.; Li, K.; Lin, S.; Li, M.; Hao, T.; Wang, T. A systematic review of factors affecting properties of thermal-activated recycled cement. *Resour. Conserv. Rec.* **2022**, *185*, 106432. [CrossRef]
20. Piao, R.; Oh, T.; Kim, G.; Choi, H.; Banthia, N.; Yoo, D. Enhanced microstructure and mechanical properties of cementless ultra-high-performance fiber-reinforced alkali-activated concrete with silicon dioxide nanoparticles. *Constr. Build. Mater.* **2023**, *398*, 132514. [CrossRef]
21. Rashad, A.; Ezzat, M.; ElNagar, A. El-Nashar M. Valorization of limestone powder as an additive for fly ash geopolymer cement under the effect of the simulated tidal zone and seawater attack. *Constr. Build. Mater.* **2023**, *369*, 130616. [CrossRef]
22. Farooq, F.; Ji, X.; Javed, M.F.; Akbar, A.; Shah, M.I.; Aslam, F.; Alyousef, R. Geopolymer concrete as sustainable material: A state of the art review. *Constr. Build. Mater.* **2021**, *306*, 124762. [CrossRef]
23. Thomas, B.S.; Yang, J.; Mo, K.H.; Abdalla, J.A.; Hawileh, R.A.; Ariyachandra, E. Biomass ashes from agricultural wastes as supplementary cement-based materials or aggregate replacement in cement/geopolymer concrete: A comprehensive review. *J. Build. Eng.* **2021**, *40*, 102332.
24. Hossain, S.S.; Roy, P.K.; Bae, C.J. Utilization of waste rice husk ash for sustainable geopolymer: A review. *Constr. Build. Mater.* **2021**, *310*, 125218. [CrossRef]
25. Zhang, P.; Wang, K.; Wang, J.; Guo, J.; Hu, S.; Ling, Y. Mechanical properties and prediction of fracture parameters of geopolymer/alkali-activated mortar modified with PVA fiber and nano-SiO_2. *Ceram. Int.* **2020**, *46*, 20027–20037. [CrossRef]
26. Wang, H.; Wang, L.; Shen, W.; Cao, K.; Sun, L.; Wang, P.; Cui, L. Compressive strength, hydration and pore structure of alkali-activated slag mortars integrating with recycled concrete powder as binders. *KSCE J. Civ. Eng.* **2022**, *2*, 26. [CrossRef]
27. Gao, Z.; Zhang, P.; Wang, J.; Wang, K.; Zhang, T. Interfacial properties of geopolymer mortar and concrete substrate: Effect of polyvinyl alcohol fiber and nano-SiO2 contents. *Constr. Build. Mater.* **2022**, *315*, 125735. [CrossRef]

28. Liu, M.; Wang, C.; Wu, H.; Yang, D.; Ma, Z. Reusing recycled powder as eco-friendly binder for sustainable GGBS-based geopolymer considering the effects of recycled powder type and replacement rate. *J. Clean. Prod.* **2022**, *364*, 132656. [CrossRef]
29. Ulugl, H.; Kul, A.; Yldrm, G.; Ahmaran, M.; Aldemir, A.; Figueira, D.; Ashour, A. Mechanical and microstructural characterization of geopolymers from assorted construction and demolition waste-based masonry and glass. *J. Clean. Prod.* **2021**, *280*, 124358. [CrossRef]
30. Yldrm, G.; Kul, A.; Zelikci, E.; Ahmaran, M.; Ashour, A. Development of alkali-activated binders from recycled mixed masonry originated waste. *J. Build. Eng.* **2021**, *33*, 101690. [CrossRef]
31. Ulugol, H.; Gunal, M.F.; Yaman, I.O.; Yildirim, G. Sahmaran, Mustafa, Effects of selfhealing on the microstructure, transport, and electrical properties of 100% construction-and demolition-waste-based geopolymer composites. *Cem. Concr. Compos.* **2021**, *121*, 104081. [CrossRef]
32. Dadsetan, S.; Siad, H.; Lachemi, M.; Sahmaran, M. Extensive evaluation on the effect of glass powder on the rheology, strength, and microstructure of metakaolin-based geopolymer binders. *Constr. Build. Mater.* **2021**, *268*, 121168. [CrossRef]
33. Mahmoodi, O.; Siad, H.; Lachemi, M.; Dadsetan, S.; Sahmaran, M. Development and characterization of binary recycled ceramic tile and brick wastes-based geopolymers at ambient and high temperatures. *Constr. Build. Mater.* **2021**, *301*, 124138. [CrossRef]
34. Aydin, E.; Arel, H.S. Characterization of high-volume fly-ash cement pastes for sustainable construction applications. *Constr. Build. Mater.* **2017**, *157*, 96–107. [CrossRef]
35. *GB/T 50082-2009*; Standard for Test Methods of Long-Term Performance and Durability of Ordinary Concrete. Ministry of Housing and Urban-Rural Development of the People's Republic of China and General Administration of Quality Supervision, Inspection and Quarantine of the People's Republic of China: Beijing, China, 2009. (In Chinese)
36. Albitar, M.; Ali, M.M.; Visintin, P.; Drechsler, M. Durability evaluation of geopolymer and conventional concretes. *Constr. Build. Mater.* **2017**, *136*, 374–385. [CrossRef]
37. Wang, Y.; Cao, Y.; Zhang, P.; Ma, Y.; Zhao, T.; Wang, H.; Zhang, Z. Water absorption and chloride diffusivity of concrete under the coupling effect of uniaxial compressive load and freeze–thaw cycles. *Constr. Build. Mater.* **2019**, *209*, 566–576. [CrossRef]
38. Wang, K.; Zhang, P.; Guo, J.; Gao, Z. Single and synergistic enhancement on durability of geopolymer mortar by polyvinyl alcohol fiber and nano-SiO_2. *J. Mater. Res. Technol.* **2021**, *15*, 1801–1814. [CrossRef]
39. Huseien, G.F.; Sam, A.R.M.; Shah, K.W.; Mirza, J. Effects of ceramic tile powder waste on properties of self-compacted alkali-activated concrete. *Constr. Build. Mater.* **2020**, *236*, 117574. [CrossRef]
40. Halit, Y.; MertYücel, Y.; Serdar, A. Mechanical properties of reactive powder concrete containing mineral admixtures under different curing regimes. *Constr. Build. Mater.* **2009**, *23*, 639–648.
41. Huo, W.; Zhu, Z.; Chen, W.; Zhang, J.; Kang, Z.; Pu, S.; Wan, Y. Effect of synthesis parameters on the development of unconfined compressive strength of recycled waste concrete powder-based geopolymers. *Constr. Build. Mater.* **2021**, *292*, 123264. [CrossRef]
42. Mahmoodi, O.; Siad, H.; Lachemi, M.; Sahmaran, M. Synthesis and optimization ofbinary systems of brick and concrete wastes geopolymers at ambient environment. *Constr. Build. Mater.* **2021**, *276*, 122217. [CrossRef]
43. Zhang, D.; Jaworska, B.; Zhu, H.; Dahlquist, K.; Li, V. Engineered Cementitious Composites (ECC) with limestone calcined clay cement (LC3). *Cem. Concr. Compos.* **2020**, *114*, 103766. [CrossRef]
44. Li, X.; Lv, X.; Zhou, X. Upcycling of waste concrete in eco-friendly strain-hardening cementitious composites: Mixture design, structural performance, and life-cycle assessment. *J. Clean. Prod.* **2022**, *330*, 129911. [CrossRef]
45. Sandanayake, M.; Gunasekara, C.; Law, D.; Zhang, G.; Setunge, S. Greenhouse gas emissions of different fly ash based geopolymer concretes in building construction. *J. Clean. Prod.* **2018**, *204*, 399–408. [CrossRef]
46. Tan, J.; Cai, J.; Li, X.; Pan, J.; Li, J. Development of eco-friendly geopolymers with ground mixed recycled aggregates and slag. *J. Clean. Prod.* **2020**, *256*, 120369. [CrossRef]
47. He, X.; Zheng, Z.; Yang, J.; Su, Y.; Wang, T.; Strnadel, B. Feasibility of incorporating autoclaved aerated concrete waste for cement replacement in sustainable building materials. *J. Clean. Prod.* **2020**, *250*, 119455. [CrossRef]
48. Guo, F.; Peng, Z.; Dai, J. Calcined sodium silicate as solid base catalyst for biodiesel production. *Fuel Process. Technol.* **2010**, *91*, 322–328. [CrossRef]
49. Ruan, H.; Wu, S.; Chen, X. Capturing CO_2 with NaOH solution from reject brine via an integrated technology based on bipolar membrane electrodialysis and hollow fiber membrane contactor. *J. Chem. Eng.* **2022**, *450*, 138095. [CrossRef]
50. Liu, X.; Liu, L.; Lyu, K.; Li, T.; Zhao, P.; Liu, R.; Shah, S.P. Enhanced early hydration and mechanical properties of cement-based materials with recycled concrete powder modified by nano-silica. *J. Build. Eng.* **2022**, *50*, 104175. [CrossRef]
51. Wu, H.; Yang, D.; Ma, Z. Micro-structure, mechanical and transport properties of cementitious materials with high-volume waste concrete powder and thermal modification. *Constr. Build. Mater.* **2021**, *313*, 125477. [CrossRef]
52. Cantero, B.; Bravo, M.; De Brito, J.; Del Bosque, I.S.; Medina, C. Water transport and shrinkage in concrete made with ground recycled concrete-additioned cement and mixed recycled aggregate. *Cem. Concr. Compos.* **2021**, *118*, 103957. [CrossRef]
53. Zhang, D.; Zhang, S.; Huang, B.; Yang, Q.; Li, J. Comparison of mechanical, chemical, and thermal activation methods on the utilisation of recycled concrete powder from construction and demolition waste. *J. Build. Eng.* **2022**, *61*, 105295. [CrossRef]